Eur. Phys. J. B **45**, 547–554 (2005)
DOI: 10.1140/epjb/e2005-00210-8

THE EUROPEAN PHYSICAL JOURNAL B

Melting evolution and diffusion behavior of vanadium nanoparticles

Wangyu Hu[a], Shifang Xiao, Jianyu Yang, and Zhi Zhang

Department of Applied Physics, Hunan University, Changsha 410082, China

Received 17 November 2004
Published online 13 July 2005 –

Abstract. Molecular dynamics calculations have been performed to study the melting evolution, atomic diffusion and vibrational behavior of bcc metal vanadium nanoparticles with the number of atoms ranging from 537 to 28475 (diameters around 2–9 nm). The interactions between atoms are described using an analytic embedded-atom method. The obtained results reveal that the melting temperatures of nanoparticles are inversely proportional to the reciprocal of the nanoparticle size, and are in good agreement with the predictions of the thermodynamic liquid-drop model. The melting process can be described as occurring in two stages, firstly the stepwise premelting of the surface layer with a thickness of 2–3 times the perfect lattice constant, and then the abrupt overall melting of the whole cluster. The heats of fusion of nanoparticles are also inversely proportional to the reciprocal of the nanoparticle size. The diffusion is mainly localized to the surface layer at low temperatures and increases with the reduction of nanoparticle size, with the temperature being held constant. The radial mean square vibration amplitude (RMSVA) is developed to study the anharmonic effect on surface shells.

PACS. 61.46.+w Nanoscale materials: clusters, nanoparticles, nanotubes, and nanocrystals – 65.80.+n Thermal properties of small particles, nanocrystals, nanotubes – 66.30.Pa Diffusion in nanoscale solids

1 Introduction

Nanoparticles play an important role in understanding the transition from the microscopic to the macroscopic. As the material dimensions reduce to the nanoscale, they exhibit a series of unique thermodynamic properties. The decrease in the melting temperature of metal particles with the reduction of their size has been found theoretically and experimentally [1–16]. The main causation for this is the high surface to volume ratio for small particles, which as a consequence of the improved free energy at the particle surface results in a decrease of the melting point. Some thermodynamic models give reasonable predictions of the melting temperatures of low dimension systems [2,3], but they are unable to give the details of the melting process, especially for the premelting behavior on the surface. In past decades, the molecular dynamics simulations on particles mainly focus on clusters of tens to several hundreds of atoms [7–16]. The melting behaviors of clusters have special properties, such as the melting point of a small tin cluster being markedly higher than that of bulk material [7], a solid-to-solid structural transformation precursor to the melting transition for Au clusters [8] and dynamics coexistence states in the vicinity of melting for some rare-gas clusters [4]. A study of the melting of bimetallic Cu-Ni nanoclusters using molecular dynamics simulations [17] indicated differential melting of the external layers, but in this case the Cu segregating to the surface essentially has a lower melting point than Ni for their conventional polycrystals. Rossi et al. [18] found that the Ag-Ni and Ag-Cu clusters with polyicosahedral core-shell structure (an inner Ni or Cu core and an Ag external shell) melted at considerably higher temperatures than pure Ag, Cu and Ni clusters in the same size range, that is to say the external layer stabilizes the clusters. For different types, as well as compositions and sizes of particles, the melting behaviors present similarities in some aspects, and at the same time have their own special characteristics.

Vanadium is a refractory metal, using molecular dynamics Sorkin et al. [19] studied the melting of bulk vanadium from mechanical and thermodynamic views. The thermodynamic investigation of the particles has important technological implications. In the present paper, we have studied the melting evolution and diffusion behavior of vanadium nanoparticles using molecular dynamics calculations with the modified analytic embedded-atom method (MAEAM) improved by our group. The whole melting process is traced from the changing of the local structure and the atomic energy. According to the structural characteristics of spherical nanoparticles, the radial mean square vibrational amplitude (RMSVA) is developed to investigate the anharmonic effect on the surface.

[a] e-mail: wangyuhu2001cn@yahoo.com.cn

Table 1. Model parameters for V.

F_0/eV	n	α/μeV	k_{-1}/eV	k_0/eV	k_1/eV	k_2/eV	k_3/eV	k_4/eV
3.282	0.750	−10.489	27.11	−136.60	281.98	−293.16	150.69	−30.31

2 Theory and simulation

2.1 Modified analytic embedded atom method

Considering the hypothesis of linear superposition of atomic electronic density and the inability to treat elements with negative Cauchy pressure, our group introduced a modified term in the atomic potential expression and reconstructed the pair potential function. These MAEAM potentials have already been successfully applied for the modeling of surfaces, point defects and thermodynamic properties [20–22].

The basic equations are

$$E_{tot} = \sum E_i \tag{1}$$

$$E_i = \frac{1}{2}\sum_{j\neq i}\phi(r_{ij}) + F(\rho_i) + M(P_i) \tag{2}$$

where E_{tot} and E_i are the total energies of the model system and a single atom, respectively, r_{ij} is the separation distance between atoms i and j, $\phi(r_{ij})$ is the pair potential as a function of the distance r_{ij}, $F(\rho_i)$ is the embedding energy to embed atom i in an electron densityρ_i, and $M(P_i)$ is the modified term, which describes the energy change caused by the nonspherical distribution of electrons and deviation from the linear superposition of atomic electronic density. The functions of $\phi(r_{ij})$, $F(\rho_i)$ and $M(P_i)$ take the following forms.

$$\phi(r_{ij}) = \sum_{l=-1}^{4} k_l \left(\frac{r_{ij}}{r_1}\right)^l \tag{3}$$

$$F(\rho_i) = -F_0\left[1 - n\ln\left(\frac{\rho_i}{\rho_e}\right)\right]\left(\frac{\rho_i}{\rho_e}\right)^n \tag{4}$$

$$M(P_i) = \alpha\left\{1 - \exp\left[-10000.0\left(\ln\left(\frac{P_i}{P_e}\right)\right)^2\right]\right\} \tag{5}$$

where r_1 is the first-neighbor distance in the equilibrium state, ρ_i is the electron density induced at site i by all other atoms in the system, and P_i is the second order item of electron density. ρ_e and P_e correspond to their equilibrium values respectively.

$$\rho_i = \sum_{j\neq i} f(r_{ij}) \tag{6}$$

$$P_i = \sum_{j\neq i} f^2(r_{ij}) \tag{7}$$

where $f(r_{ij})$ is the electron density distribution function of an atom and is taken as

$$f(r_{ij}) = f_e\left(\frac{r_1}{r_{ij}}\right)^{4.5}\left(\frac{r_{ce} - r_{ij}}{r_{ce} - r_1}\right)^2 \tag{8}$$

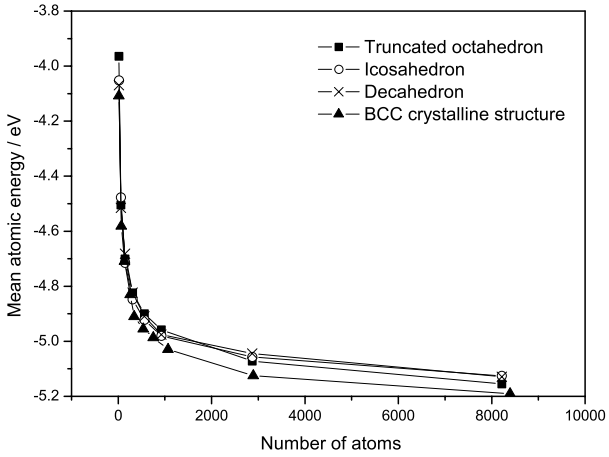

Fig. 1. Mean atomic energy vs. the number of atoms for truncated octahedron, icosahedron, decahedron and extracted spherical nanoparticles from bcc crystalline structure.

where f_e is taken to be 1.0. In the present model, the atomic interactions up to second neighbor distances are considered, and $\phi(r_{ij})$ is truncated between the second and third neighbors. The electron density function $f(r_{ij})$ is truncated at $r_{ce} = 1.559a_0$, where a_0 is the lattice constant.

The model parameters are determined by fitting the physical properties of vanadium, such as cohesive energies, vacancy formation energy, and elastic constants. The calculated model parameters for vanadium are listed in Table 1.

2.2 Simulation procedure

The initial configurations of spherical nanoparticles, with 537, 1067, 2891, 8393, 14361 and 28475 atoms, are extracted from a perfect crystal, and all of the atoms are located on their lattice positions. The stable structure at 0 K is obtained through the initial configurations annealed fully at $T = 300$ K and then cooled to $T = 0$ K at a cooling rate of 50 K/100 ps. The annealed microstructure is almost the same as the initial configuration except for the relaxed surface atoms. Considering the competitive structural motifs in metallic nanoclusters with the same number of atoms, the variation of mean atomic energy with the number of atoms with different structural motifs, such as truncated octahedron, icosahedron, decahedron and extracted spherical nanoparticles from bcc crystalline structure, is shown in Figure 1. It is clearly shown that the extracted spherical nanoparticles are the most stable, from the viewpoint of energy, for clusters with the number of atoms ranging from 537 to 28475. For the investigation of melting evolution and distinctive surface properties, four

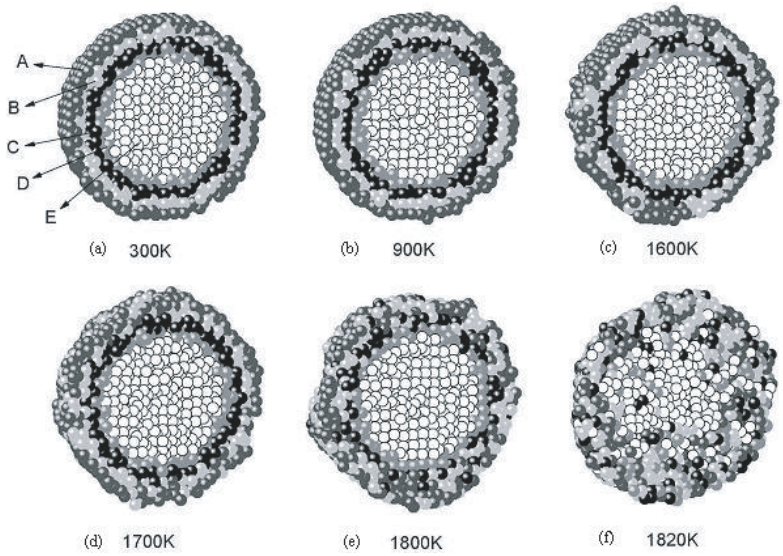

Fig. 2. Section snapshot views of the MD sample with $N = 8393$ ($D \approx 6$ nm) at a series of temperatures during heating.

spherical shell regions with the same thickness of a_0 are divided and labeled as A, B, C, D, starting from the outmost shell, and the remaining core is labeled as E (as shown in Fig. 2a) and analyzed respectively.

During heating in order to get an energy-optimized structure at a given temperature, molecular dynamics calculations are carried out under constant volume and constant temperature controlled by a Nose-Hoover thermostat [23,24] (NVT ensemble) without periodic boundary conditions. In integration of the classic equations of motion we used a fourth-order Gear predictor-corrector algorithm with a time step of 1 fs and the linear and angular momenta were eliminated at each temperature. For each nanoparticle, the system is relaxed 50 000 time steps (50 ps) at various temperatures far from the melting region, while at several points near the melting point (T_m) the systems are relaxed for 100000 time steps (100 ps), and all of the statistical data are collected from further 50000 MD time steps.

3 Result and discussion

3.1 The melting process and evolution

The experimental observation of the melting phenomena on a particle is just the surface liquid skin resulted by surface premelting. Using molecular dynamic simulation, the melting process and melting mechanism of nanoparticles can be analysized. Figure 2 shows section snapshots of the nanoparticle with 8393 atoms at several typical temperatures during heating, and the corresponding radial distribution functions (RDF) for each spherical shell at these temperatures are shown in Figure 3, where the RDF is defined as $g(r) = \langle n(r)/(\rho_0\, 4\pi r^2 \Delta r)\rangle$, $n(r)$ is the number of atoms in a shell of width Δr at distance r, ρ_0 is the mean atom density for the perfect lattice and the angular brackets denote averaging over atoms. At a temperature of 1600 K, the RDF of the outmost shell, labeled as A, begins to approach the character of the liquid structure, local disordered regions appear on the surface layer (as shown in Fig. 2c and Fig. 3c). As the temperature increases to 1700 K, shell A becomes disordered, like a liquid, and shell B begins to incline to liquid disorder (as shown in Fig. 2d and Fig. 3d). As the temperature increases to 1800 K, shell B turns into liquid and shell C begins to incline to full disorder, and a consecutive liquid film attaches to the inner core which still remains as an ordered solid (as shown in Fig. 2e and Fig. 3e). After the temperature increases to 1820 K, all of the outer shells and the inner core behave as though fully disordered (as shown in Fig. 2f and Fig. 3f). The evolution of atomic configurations with temperature indicates that the premelting on the surface layers is a step-by-step process from the outmost surface. When the temperature approaches the melting point, the inner core melts suddenly, just as in the conventional crystalline. As mentioned above, a solid-to-solid structural transformation occurs as a precursor to the melting transition for small Au clusters [8], but in present studies, the RDF analysis shows that there is no structural transformation prior to melting in bcc vanadium clusters.

The relations between the mean atomic energy and temperature for six kinds of nanoparticles and bulk vanadium are shown in Figure 4. Except near the melting point regime, the average atomic energies of these systems increase approximately linearly with the increase in temperature. The typical signature of melting obtained from the caloric curves is a jump in energy $\varepsilon(T)$. It is obvious from Figure 4 that there is no unique temperature corresponding to the melting transition on the caloric curves. The midpoint of a jump was selected as the melting point in the present work. The obtained melting point of bulk vanadium is about 2169 K, it is close to the experimental value

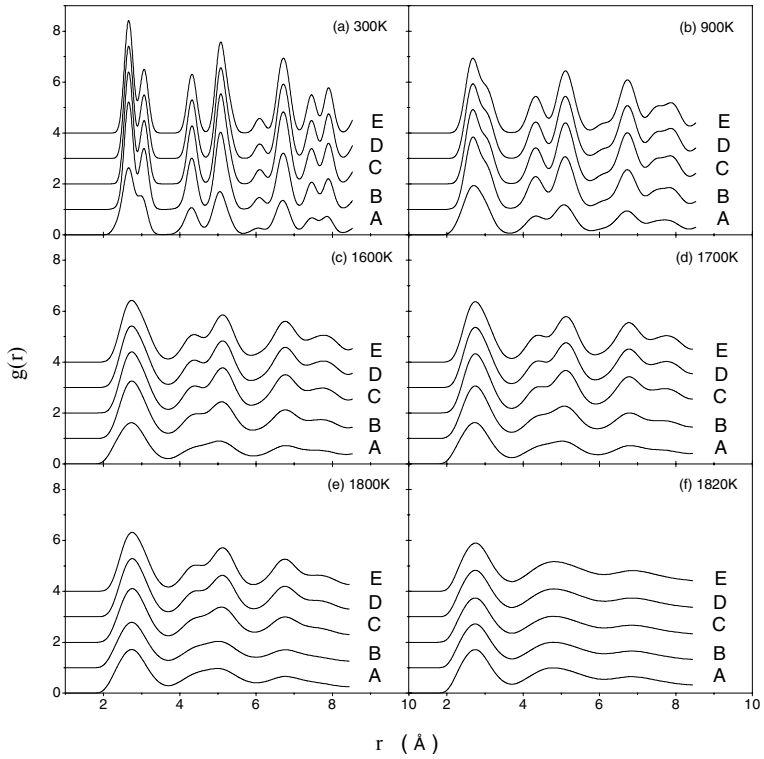

Fig. 3. The radius distribution function evolution with the temperature for the nanoparticle with number of atoms 8393, the A, B, C, D and E correspond to different spherical shell regions as indicated in Figure 1.

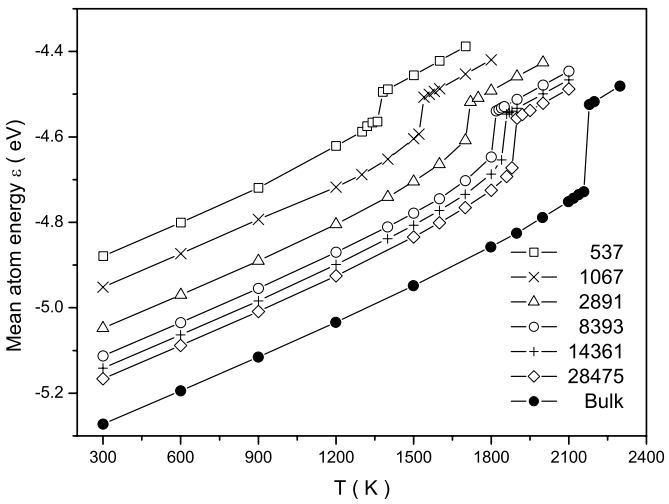

Fig. 4. The mean atomic energy as a function of temperature for six different nanoparticles and bulk. Numbers labeling the curves are the number of atoms in the MD cell. The jumps in the curves indicate melting transitions.

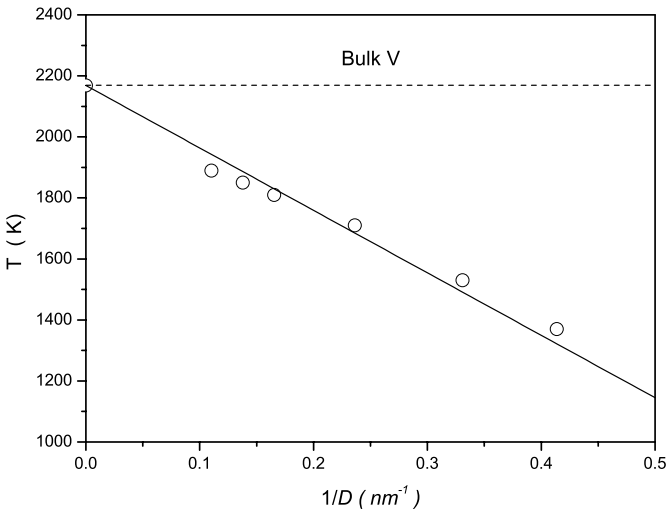

Fig. 5. Melting point vs. the reciprocal of nanoparticle diameter. The dashed line represents the melting point of bulk vanadium. The solid line is the result calculated from the thermodynamic model $T_m = T_{mb}(1 - \beta/d)$ [2], (T_{mb} the melting of bulk, d the particle diameter, $\beta = 0.944$).

of T_m = 2183 K [25]. The dependence of the obtained melting point on nanoparticle size is shown in Figure 5. The melting point decreases linearly with the reciprocal of the nanoparticle size. This result is in good agreement with the prediction from the liquid-drop model [2]. The thermodynamic theory gives a detailed description using the concept of surface energy for the decline of melting temperature of nanoparticle [2,3]. It is well known that melting is a process where the bonds between atoms are broken. Comparing with the perfect crystalline, about half of the bonds of the surface atoms are dangling. For particles of nanoscale size, the ratio of surface atoms to volume atoms increases rapidly as the particle size decreases, and

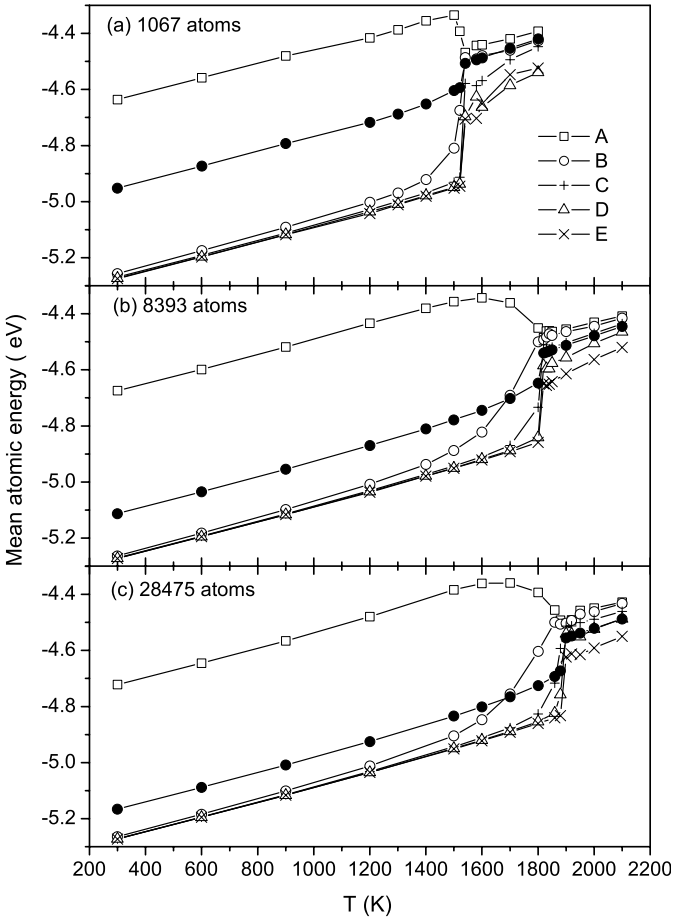

Fig. 6. The mean atomic energy of different spherical shells and system vs. temperature for the nanoparticles with 1067, 8393 and 28475 atoms. The filled circle denotes the mean atomic energy of the whole system.

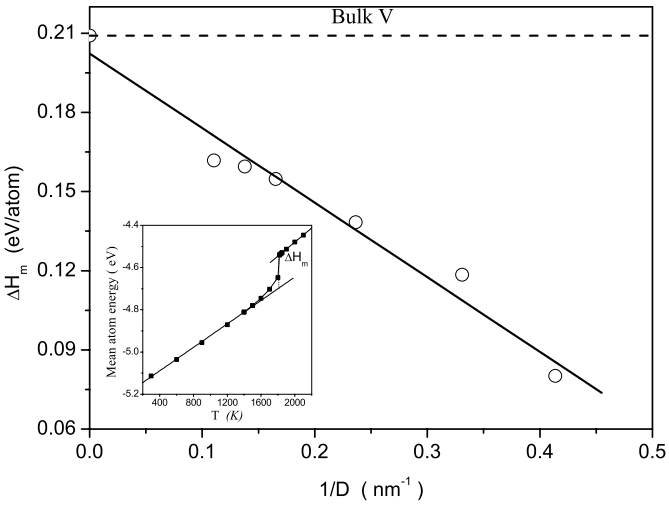

Fig. 7. The heat of fusion vs. the reciprocal of nanoparticle diameter. The dashed line represents the heat of fusion of bulk vanadium. The insert figure shows the determination of the heat of fusion.

results in the surface energy increasing and the melting point decreasing pronouncedly.

The atomic energy is closely related to its surrounding structure, and then the structural transformation, as discussed above, can be analyzed from the point of view of atomic energy. Figure 6 shows the temperature dependence of mean atomic energy for different spherical shells and the whole system. It shows for all samples that the mean atomic energy of shell A is quite different from the other shells, which indicates that the surface atoms are much more active than the other atoms. In contrast with the inner core, the difference in the temperature dependence of mean atomic energy for the outer shells concentrates on the outermost 2 shells for the sample with 1067 atoms, the outmost 3 shells for the sample with 8393 atoms, and there exists little difference from the core until the fourth outer shell for the sample with 28475 atoms. This demonstrates that the thickness of the liquid skin overlaying the inner core is discrepant as the particle size increases. Interestingly, as the energy of the second outer shell, B, increases rapidly, the mean atomic energy of the outmost spherical shell, A, decreases with the increase in temperature near the melting point. With the elevation in temperature, the melting continues to the inside shells from the outmost shell, many atoms in this shell diffuse into the inside shell and have lower energy. However, the inner core of the nanoparticle is still solid at this temperature as shown in the caloric curves. At the melting temperature, the jump on the caloric curves of the inner core and the system occurs simultaneously. This also agrees with the stepwise premelting on the surface layers and the sudden melting behavior of the nanoparticle.

As discussed above, the melting of nanoparticles is composed of two stages: the stepwise premelting on the surface layers and the sudden melting in the core. Correspondingly, the calculation of the heat of melting should comprise of two parts. In the present paper, we linearly fit the low temperature and above melting point regions of the caloric curves, respectively, and take the interval between these two lines at melting point as the heat of fusion (as shown in the inset figure of Fig. 7). The obtained heat of fusion of bulk vanadium is about 20.2 kJ/mole, which is close to the experimental value of ΔH_m = 20.9 kJ/mole [25]. Figure 7 shows the size dependence of the heat of fusion. It is obvious that the heat of melting for the nanoparticles is much lower than that of the bulk vanadium and also decreases linearly with the reciprocal of the nanoparticle size.

3.2 Diffusion behavior

The diffusion coefficients of the atoms was calculated by using the Einstein equation

$$D = (1/6)(1/t)\langle[r(t) - r(0)]^2\rangle \quad (9)$$

where D is the diffusion coefficient, t is the diffusion time, and r is the position of the atoms. The mean square

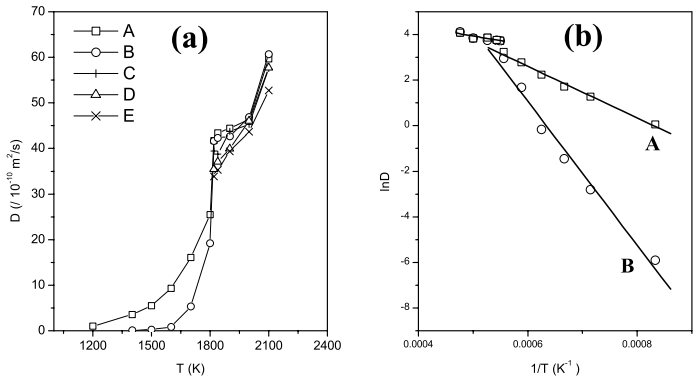

Fig. 8. (a) Temperature dependence of the diffusion coefficient for different shells for the sample with 8393 atoms; (b) Arrhenius's plot for outer shells A and B in (a).

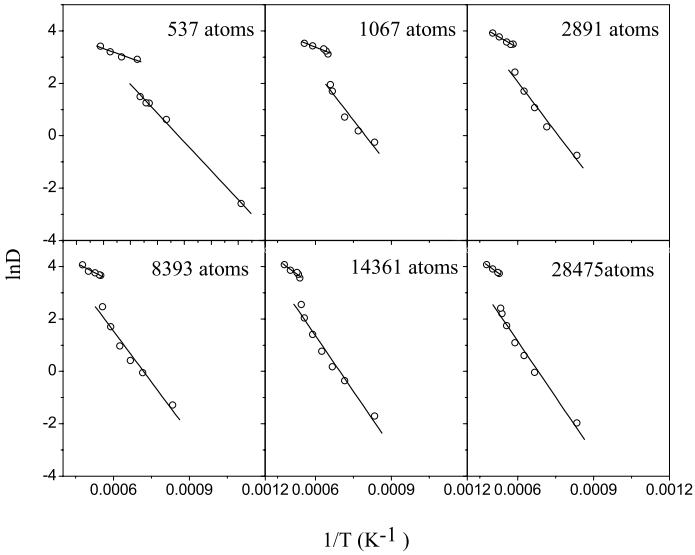

Fig. 9. Arrhenius's plot for the average diffusion coefficient of nanoparticles with various diameters at different temperatures.

displacement $\langle [r(t) - r(0)]^2 \rangle$ for the atoms was calculated by

$$\langle [r(t) - r(0)]^2 \rangle = (1/n_i) \sum_i [r_i(t) - r_i(0)]^2. \qquad (10)$$

As shown in Figure 8a, for the sample with 8393 atoms, the diffusion is mainly localized to the surface layers at low temperature, and the diffusion coefficient increases rapidly with increasing temperature. Consisting with the above discussions, the atoms on the surface layers have a very high diffusion coefficient. When the temperature approaches melting point, there is a sudden increase in the diffusion coefficient for all of the shells. Furthermore, even above the melting temperature, the outer shells have higher diffusion coefficients than the inner core. Other samples exhibit a similar diffusion behavior.

In general, the temperature dependence of the diffusion coefficient can be expressed as Arrhenius's relation:

$$D = D_0 \exp\left(-\frac{Q}{RT}\right) \qquad (11)$$

where D_0 is the prefactor of diffusion coefficient, R is the gas constant and Q is the activation energy for diffusion. Figure 8b shows the Arrhenius's plot of $\ln D$ to $1/T$ for Figure 8a for the outer shells A and B. As discussed above, the premelting on the surface layers is a step-by-step process from the outmost surface to the inner core, and the inner core melts suddenly at melting temperature. Thus, the diffusion is not obvious for inner shells E, D, and C, which indicates that the diffusion mechanism for nanoparticles is dominated by surface diffusion. Two stages for diffusion can clearly be seen for shells A and B. One stage represents the diffusion process below the melting point, and the other represents the diffusion process above the melting point. Because the diffusion coefficients of other shells are too small at low temperatures, it is rather difficult to determine the activation energy for the diffusion of these shells. The obtained activation energies for diffusion from Figure 8b are approximately 94 kJ/mole and 263 kJ/mole for shell A and shell B, respectively, which confirms that the surface atoms are more active.

Figure 9 shows the Arrhenius's plots for these nanoparticles. It reveals that the diffusion behavior of nanoparticles is dominated by the surface atoms and also shows 2 stages for the diffusion process. The diffusion activation

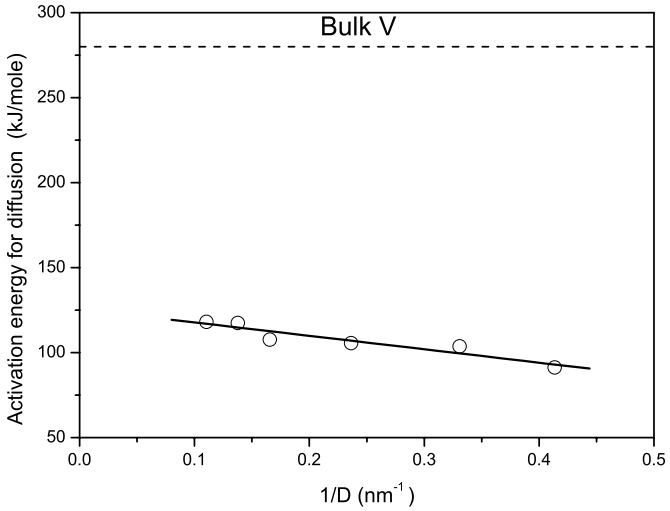

Fig. 10. Activation energy for diffusion vs. the reciprocal of nanoparticle diameter. The dashed line represents the activation energy for diffusion of bulk vanadium.

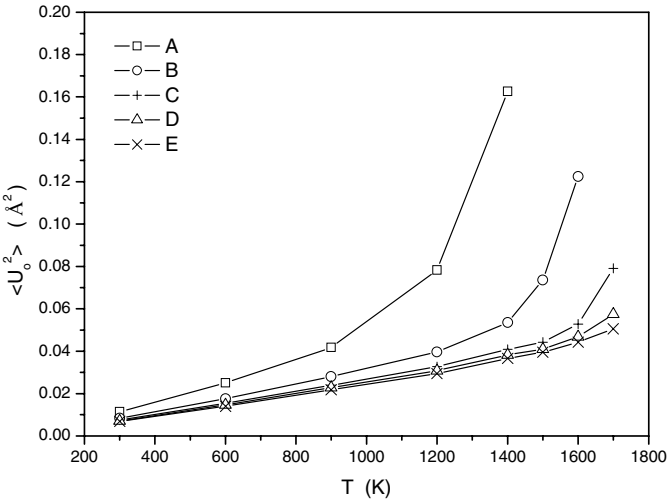

Fig. 11. Radial mean-square amplitudes of vibration $\langle U_o^2 \rangle$ for the various shells (see text) of the sample with 8393 atoms as a function of temperature.

energy for the lower temperature stage decreases with the reciprocal of the nanoparticle size as shown in Figure 10. With the reduction of nanoparticle size, the fraction of surface atoms increases and the melting point decreases, thus the diffusion activation energy decreases and the diffusion coefficient increases at the same temperature. On the other hand, the diffusion activation energy for these nanoparticles is only one third of the corresponding diffusion activation energy of bulk vanadium, $Q_{\rm bulk}$ ($Q_{\rm bulk} = 280$ kJ/mole [26]). This result indicates that diffusion is induced by the surface effect of nanoparticles.

The activity of surface atoms can be interpreted with the radial mean square vibration amplitudes (RMSVA) which is defined as:

$$\langle u_0^2 \rangle = \frac{1}{n_1} \sum_{i=1}^{n_1} \left\langle \left[\vec{r}_{i,o}\,(t) - \langle \vec{r}_{i,o}\,(t) \rangle \right]^2 \right\rangle \qquad (12)$$

where n_1 is the number of considered atoms. The particle center of mass is selected as the origin, and $\vec{r}_{i,o}$ is the radial distance relative to the center of mass.

In a harmonic system, $\langle U_o^2 \rangle$ increase linearly with increasing temperature, and therefore deviations from linearity are a measure of anharmonicity. The calculated RMSVA, shown in Figure 11 for different shells, demonstrates substantial anharmonicity at elevated temperatures, and the vibrations and anharmonic effects increase with the increment of the shell's radial distance. This result reveals that the surface effect is important for the diffusion behavior and melting properties of nanoparticles. The effects of this anharmonicity on the specific heats and thermal expansion of nanoparticles await further study.

4 Summary

In this paper, we have investigated the melting evolution, diffusion and vibrational behavior of vanadium nanopaticles with molecular dynamics simulation using an analytic embedded-atom method. It has been found that the melting point is inversely proportional to the reciprocal of the nanoparticle size and the results are in good agreement with the theoretical analysis from the liquid drop model. This proves that our MAEAM many-body potential describes the interaction between metallic atoms effectively. The evolution of atomic configuration and energy with temperature reveals that the melting process of vanadium nanoparticles can be described in two stages, the stepwise premelting from the outmost surface and the sudden melting in the inner core. The thickness of the liquid skin resulting from the surface premelting is discrepant for particles with different diameters. Owing to the two stage melting, the heat of melting for nanoparticles should involve two parts. As the particle size decreases, the heat of melt decreases correspondingly. The atomic diffusion in nanoparticles is mainly localized to the surface layers before the melting temperature and increases with the reduction of particle size at the same temperature. The diffusion activation energy for these nanoparticles is only about one third of $Q_{\rm bulk}$. The studies of the radial mean-square vibration amplitudes of spherical particles show that the surface anharmonic effect on nanoparticles is remarkable.

This work is financially supported by the NSFC (No.50371026), the Hunan Provincial Natural Science Foundation and the High Performance Computing Center of Hunan University.

References

1. Ph. Buffat, J.P. Borel, Phys. Rev. A **13**, 2287 (1976)
2. K.K. Nanda, S.N. Sahu, S.N. Behera, Phys. Rev. A **66**, 013208 (2002)
3. Q. Jiang, S. Zhang, M. Zhao, Mater. Chem. Phys. **82**, 225 (2003)
4. C.L. Cleveland, U. Landman, W.D. Luedtke, J. Phys. Chem. **98**, 6272 (1994)

5. T. Bachels, H.J. Guntherodt, R. Schafer, Phys. Rev. Lett. **85**, 1250 (2000)
6. S.J. Zhao, S.Q. Wang, D.Y. Cheng, H.Q. Ye, J. Phys. Chem. B **105**, 12857 (2001)
7. A.A. Shvartsburg, M.F. Jarrold, Phys. Rev. Lett. **85**, 2530 (2000)
8. C.L. Cleveland, W.D. Luedtke, U. Landman, Phys. Rev. Lett. **81**, 2036 (1998)
9. C.L. Cleveland, W.D. Luedtke, U. Landman, Phys. Rev. B **60**, 5065 (1999)
10. H. Lei, J. Phys: Condens. Matter. **13**, 3023 (2001)
11. L. Wang, Y. Zhang, X. Bian, Y. Chen, Phys. Lett. A **310**, 197 (2003)
12. S. Ozcelik, Z.B. Guvenc, Surf. Sci. **532-535**, 312 (2003)
13. S.L. Lai, J.Y. Guo, V. Petrova, G. Ramanath, L.H. Allen, Phys. Rev. Lett. **77**, 100 (1996)
14. L.J. Lewis, P. Jensen, J.L. Barrat, Phys. Rev. B **56**, 2248 (1997)
15. F. Baletto, A. Rapallo, G. Rossi, R. Ferrando, Phys. Rev. B **69**, 235421 (2004)
16. M. Schmidt, R. Kusche, B. von Issendorff, H. Haberland, Nature **393**, 238 (1998)
17. S.P. Huang, P.B. Balbuena, J. Phys. Chem. **106**, 7225 (2002)
18. G. Rossi, A. Rapallo, A. Fortunelli, C. Mottet, F. Baletto, R. Ferrando, Phys. Rev. Lett. **93**, 105503 (2004)
19. V. Sorkin, E. Polturak, Joan Adler, Phys. Rev. B **68**, 174102, 174103 (2003)
20. W. Hu, X. Shu, B. Zhang, Comput. Mater. Sci. **23**, 175 (2002)
21. W. Hu, M. Fukumoto, Model. Simul. Mater. Sci. Eng. **10**, 707 (2002)
22. W. Hu, H. Deng, X. Yuan, M. Fukumoto, Eur. Phys. J. B **34**, 429 (2003)
23. S. Nose, J. Chem. Phys. **81**, 511 (1984)
24. W. Hoover, Phys. Rev. A **31**, 1695 (1985)
25. *Handbook of Chemistry and Physics*, 81'st edn., edited by D.R. Lide, (CRC Press, 2000–2001)
26. R.W. Siegel, in *Proceedings of Yamada Conference on Point Defect Internations in Metals*, edited by J. Takamura, M. Doyama, M. Kiritani (University of Tokyo Press, Tokyo, 1982), p. 533